Colloids and Surfaces A 574 (2019) 188–196

Contents lists available at ScienceDirect

Colloids and Surfaces A

journal homepage: www.elsevier.com/locate/colsurfa

Blood droplets on functionalized surfaces: Chemical, roughness and superhydrophobic effects

Rodney Marcelo do Nascimento*, Ana Paula Ramos, Pietro Ciancaglini, Antônio Carlos Hernandes

University of Sao Paulo, USP, Brazil

GRAPHICAL ABSTRACT

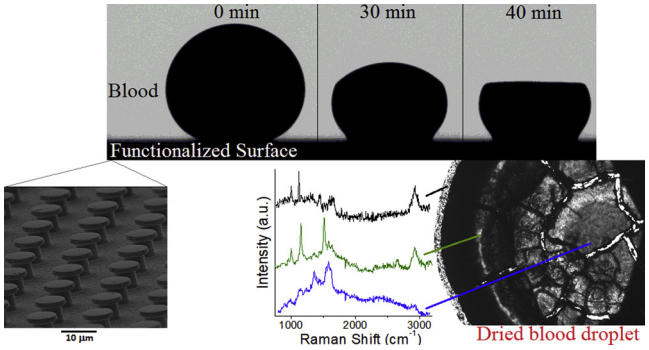

ARTICLE INFO

Keywords:
Bloodphobicity
Contact line
Contact angle
Stain rings
Blood components
Interface 3D modelling

ABSTRACT

This manuscript reports the phenomenology of blood-material interface assessed by contact angle measurements and Raman spectroscopy. In particular, chemistry, topology and superhydrophobic effects on the contact line of blood droplets were investigated by using distinct substrates: Silicon, Ti13Nb13Zr and bioinspired-like PTFE, respectively. The surfaces were functionalized through different process aiming to study the specific effects. The chemical fingerprints of the biomolecules at the blood stain rings appear to be influenced by the contact line, which in turn depends on the kind of chemical treatment. A five-fold increase in roughness parameters by a metallic thinning process leads to a hydrophilic-hydrophobic transition in the metallic substrate followed by an increase in the bloodphobicity. In order to assess the extreme in the super blood-phobic state observed in a bio-inspired surface, a simple 3D model based on thermodynamic standpoint and solid-liquid fraction has been proposed to predict optimized parameters for the substrate. Collectively, the results can offer new insights towards the objective of rational substrate design that can improve next generation blood-devices and antithrombogenic metallic implants.

1. Introduction

Blood is a vital body fluid responsible for different functions performed by a large number of cells suspended in a biological medium (plasma). A deep understanding of the interface between blood droplets and surfaces of different materials is important to both fundamental

* Corresponding author at: Sao Carlos Institute of Physics, University of São Paulo, University of São Paulo, USP, Avenida João Dagnone, 1100, Jardim Santa Angelina, CEP 13563-120, São Carlos, SP, Brazil.
E-mail address: rodney.nascimento79@gmail.com (R.M. do Nascimento).

https://doi.org/10.1016/j.colsurfa.2019.04.025
Received 11 February 2019; Received in revised form 31 March 2019; Accepted 11 April 2019
Available online 30 April 2019
0927-7757/

and applied science in the medical fields. Examples include the development of blood drop-based devices for diagnosis [1] and antithrombogenic biomaterials [2]. However, given the colloidal complexity and multi-factoriality of the whole blood-material interactions, the optimized, controllable and reproducible conditions for specific functionalities are extremely arduous to assess. Predicting any given specific parameters is also difficult and depends on abilities to obtain local information on cause-effect prevailing at the blood-material interface.

The characterization of the bloodstain ring patterns formed from dried blood droplets on substrates may be an interesting option for applications such as substrate for disease diagnosis [1,3,4]. In this way, the physical mechanisms behind the spreading-drying process of whole human blood on substrates, such as adsorption [5], imbibition [6], cracks formations [7], delamination [8] and humidity [9], have been better understood. For such medical applications, however, it is important to establish simple, fast and inexpensive methods including the substrate preparations and functionalization by chemical treatments. Beyond basic science questions regarding the chemical nature of the contact line of blood droplets on surfaces, studying the effect of simple chemical treatments of substrates (such as immersions in alkaline and acid solutions for cleaning and/or activation) on such blood-material interactions offers practical value for applied R&D towards improved next-generation biomarkers for disease diagnostics. This is the first goal of our study.

A second aspect which we investigate is the effect of the roughness of metallic titanium implants on blood droplets spreading-adhesion. Studies have focused on the materials for antithrombogenic implants which need to be able to resist the adsorption and adhesion of blood components (erythrocytes leukocytes, platelets and plasma proteins) and avoid the blood clotting process and blood coagulation [2,10–13]. Medical problems in metallic implant applications are associated with blood-material compatibility, which is a result of different biological interactions among cells, proteins and surfaces [14]. In fact, influences of the topology, from micro to nanoscale, on the quality, quantity and conformation of blood components adsorbed on surfaces is expected. In this way, gaps in the understanding of blood-topology include: (a) how much low blood spreading-adsorption-adhesion as function of increase or decrease of the roughness is essential for achieving favorable blood-surface compatibility [15]?; (b) should surface antifouling for blood adsorption be modified to prevent, for instance, platelet adhesion [16] through adjusting wettability by roughness parameters?

Another seldom-explored aspect, which we wanted to elucidate, relates to the extreme effects of Surface Wettability (SW). Although controversial, there are results showing that SW (measured by angles formed between liquid droplets and the surface) have an impact on biological interactions with surfaces, in particular, due to cell and protein interactions [17–22] which in turn, depend on topology, solid free energy and surface charge [23–28]. On the other hand, few efforts are given to clarify the impact of a superhydrophobic regime at whole blood-substrate interfaces. Physical models could predict stability at the interface considering phase fractions and the interfacial minimal energy γ_i towards the objective of rational blood-microfluidic device, biomaterial and biomarker designs. Therefore, we have hypothesized that SW is also the major indicator to achieve the local information at the blood-superhydrophobic material interface as well. In this study, the extreme of wettability regime with contact angles $\theta > 150^\circ$ was assessed by using a bioinspired hierarchical surface in order to investigate how this regime affects the blood contact line.

The need to establish a clear correlation between surface wettability and blood spreading-drying phenomenology is, thus, evident and is a major goal of this study. We have hypothesized that the quantification of the main physical parameters regarding interfacial energies associated with bio-physicochemical characteristics of the contact line is a key element to assess the blood-material interface. This manuscript reports, therefore, a study of the blood droplets on functionalized surfaces investigated by contact angle measurements and Raman spectroscopy. Section 3.1 outlines the wettability of surfaces through contact angle measurements for the determination of the equilibrium contact angle (steady-state) of all surfaces. Section 3.2 addresses the characterization of the blood components at stain rings by Raman spectroscopy. The blood components were fully described through the identification of the molecular fingerprints of the biomolecules. Section 3.3 describes the effects of simple chemical treatments on blood contact line and its molecular spectra using a Silicon substrate treated by acid and alkaline solutions. Section 3.4 describes the effect of the roughness on wetting transitions in Ti13Nb13Zr metallic substrates. Section 3.5 describes the fakir effect on high contact angle measured between blood and surfaces. Furthermore, simple modeling based on free energy minimization intermediated by a constraint equation is proposed in order to well-characterize the super-blood-hydrophobic state and predict optimized states for applications in blood devices.

2. Materials and methods

2.1. Blood samples

Human blood from a healthy volunteer was taken in Unimed-São Carlos medical center of analyses and stored in sterile tubes with anticoagulant. All experiments were performed within 8 h of donation to avoid deterioration of the liquid. Blood droplets were evaporated under a constant volume (2μL) at 22 °C. Ultra-pure water was introduced to both characterize the wetting properties of surfaces and compare with blood wettability. From the blood analysis, Pallidum is negative, as attested by serology and HBsAG, and Hepatitis C are not reactive, as attested by chemical luminescence. The protocols were approved by the ethics committee of the institution with the national registry of health (CNES) n° 5901995. Complete data of the blood used in the experiments are reported in Supplementary Table S1 (ISO 9001:2000, ANS 35403-1).

2.2. Substrates and surface functionalization

2.2.1. Silicon surfaces

In order to study the effects of chemical treatments of substrates on the blood contact line, commercial flat silicon substrates Si (100) of $5 \times 5\,mm^2$ were submitted to acid and alkaline treatments. The samples were dipped in 1 Mol HCl and NaOH solutions for 1 min and sequentially cleaned 3 times in an ultrasonic bath with acetone, isopropyl alcohol and ultrapure water (for 15 min each step), and finally dried at 50 °C for 10 min. The surfaces treated by acid and alkaline solutions, labeled as Si − HCl and Si-NaOH, respectively, were characterized by contact angle measurements, and the values were compared with a flat surface (control). The charging of the Silicon samples modified by the chemical treatments were monitored by surface zeta-potential (ζ) at pH 7.4 using a Zeta-sizer Nano ZS instrument (Malvern Instruments) coupled to a ZEN 1020 dip cell. The mobility of tracer particles in the vicinity of the charged test surface fixed in the dip-cell was monitored by using phase analysis light scattering and a simple model that describes the electroosmotic flow near the surface. The tracer particles consisted of polystyrene nanospheres (200 nm and $\zeta = -50.0$ mV, Duke Scientific Corporation) dispersed in Milli-Q water.

2.2.2. Ti13Nb13Zr surface

In order to study the topological effects of metallic implants on the blood contact line, samples of titanium alloy Ti13Nb13Zr (a candidate metallic biomaterial for bone replacement) $10 \times 20\,mm^2$ were wet ground with 280, 400 and 1200 mesh sandpapers. After cleaning in ultra-pure water, a sample was polished and labeled pol-Ti313. For the roughening of the surface, thinning process was employed and a sample was abraded by 9 μm Alumina (Al_2O_3) and labeled Ti13Nb13Zr-r1. Topographical and morphological analyses of the surfaces were performed on $25 \times 25\,\mu m^2$ ROIs to estimate the surface roughness

parameters using an atomic force microscope (AFM, Shimadzu SPM instrument version 2.0) under dry conditions. The analyses were performed in contact mode using 200 μm 0.15 N/m triangular silicon nitride cantilevers with gold coated tips (OMCL-TR800PSA, Olympus, Japan). Image analyses were performed using the manufacturer SPM-Offline software (Version 3.304, Shimadzu). From surface profiles, the following roughness parameters $R_{parameters}$ were obtained: average roughness R_a, root mean squared R_q, maximum peak height R_p, maximum valley depth R_v, ten-point height R_z and five highest peaks and lowest valleys R_{zjis} Statistical data on the surface area were obtained from different regions of each sample.

2.2.3. Bio-inspired mushroom-like surface

In order to investigate the extreme of hydrophobic regime on the blood contact line, a silicon substrate was decorated with micrometer-sized mushroom-like pillars etched to obtain a regular square lattice (an image of the regular microstructure is provided in the abstract figure). Such a specific geometry has been chosen to ensure the enhanced stability of the superhydrophobic state throughout the drop evaporation by taking advantage of the reentrances. The surface was rendered hydrophobic followed by a decrease of the free energy through the deposition of fine silane-like or PTFE-like coatings from a prior C_4F_8 plasma treatment and labeled Mus-Si. Detailed information on the characteristics and wetting properties of the bio-inspired superhydrophobic surface has been provided elsewhere [29]. The results were used for identification of common blood-surface characteristics for mathematical modeling. The writing of the equations and the graphical analysis were performed by Maple 18 and Origin 8.5 softwares, respectively.

2.3. Drop evaporation and wetting characterization

Evaporation of the blood droplets and contact angle measurements were carried out through the standard sessile drop method on a KSV CAM 200 tensiometer/goniometer. For each experiment, blood droplets (˜ 2 μL in volume) were gently deposited on the functionalized surfaces at 22 °C in a glass chamber using a calibrated microsyringe. Side-view images of the drops were recorded with a CCD camera for subsequent contact angle and contact radius measurements. The measurements were performed optically with an accuracy of 1°. At least three measurements were taken in random different regions of interest (ROI) in each sample. To avoid any perturbation from external flux, the chamber remained closed during the experiments. The contact line was obtained from the contact angle θ and interfacial area S_i measurements as a function of the time using CAM2008 software, immediately after disconnection of the drop and needle. Ultra-pure water droplets were placed on the surface under the same experimental conditions. The contact line of the water drop was advanced and receded by adding and withdrawing a small volume (~ 2 μL) of fluid. The rupture angle θ_{rup} was measured immediately before the rupture of the meniscus.

2.4. Confocal raman spectroscopy

The blood stain rings formed on the substrate after evaporation were investigated by vibrational spectroscopy and correlated to wetting properties of the surfaces. The spectra and the Raman spectral mapping were obtained by a WITec alpha 300 microscope equipped with linear stage, piezo-driven, Nikon 20x and 100x objective lenses and polarized laser operating with a wavelength of 514 nm. The Raman light was detected by a high-sensitivity, back-illuminated spectroscopic CCD behind a 600 grooves/mm grating. The integration time for each point was 0.5 s and measurements were performed at room temperature.

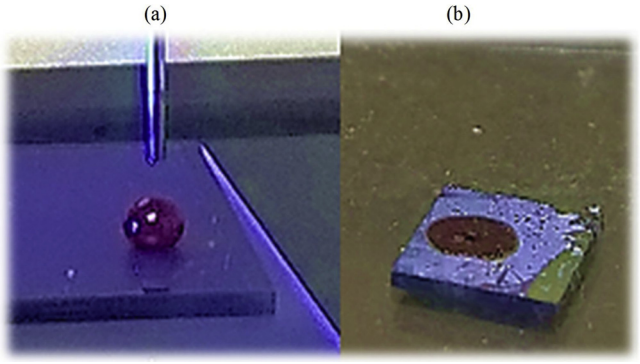

Fig. 1. Comparison between different wettability regimes. Images of blood droplets of 2 μL on superhydrophobic (a) and high hydrophilic (b) surfaces.

3. Results and discussion

3.1. Wetting characterization

The characterization of the wetting regimes at the blood-material interface on different substrates with specific surface functionalization process resulted in a variable spectrum of SW, affecting both hydrophilicity and hydrophobicity, and therefore blood spreading. In a preliminary study, we have observed that a high hydrophilic Natural Rubber-based considerably increased the wetting of the blood droplets with contact angle $\theta < 20°$ [30]. We attributed such properties to adsorption ability of proteins and some chemical components in the human blood. In this study, we have assessed the opposite wettability regime. Fig. 1 illustrates the two extremes that are mentioned with images of blood phobic and bloodphilic regimes.

A quantitative study in SW was conducted through the measurements of the contact angle θ and interfacial area S_i at the blood-substrate interface. Typical results on commercial Silicon substrate surfaces are shown in Fig. 2. Two distinct regimes can be identified: (i) the formation of the new blood-surface interface began with a decrease in θ and an increase in S_i attributed to the spread of the drop and accommodations of the contact line and (ii) the contact line reaches the steady-state characterized by a maxima interfacial area S_i. We refer to the optimal contact angle θ^* as the major indicator of the SW, which is the first value of θ obtained at a time when $\delta S_i / \delta t = 0$ in the curve over time. Thereon, the decreasing of the values of θ and/or interfacial area is conditioned to the natural evaporation process.

Table 1 shows the wetting characterization of all surfaces used in

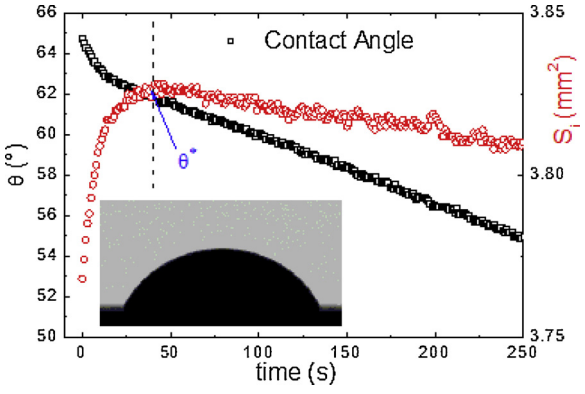

Fig. 2. Temporal evolution of contact angle θ (black) and interfacial area S_i (red) of blood droplets at 22 °C on Silicon substrate. The optimal contact angle $\theta^* = 62°$ obtained from the maximum value of blood-surface interfacial area S_i after spreading on surface is indicated in the graph. Inset: respective profile of drop on surface. (For interpretation of the references to colour in this figure legend, the reader is referred to the web version of this article).

Table 1
Wetting characterization of the functionalized surfaces: optimal contact angles of the blood θ_B^* and water θ_W^* droplets.

	Si	Si-HCl	Si-NaOH	Pol-Ti1313	Ti1313- r1	Mus-PTFE
θ_B^* (°)	62 ± 1	58 ± 1	69 ± 2.5	63 ± 2.5	100 ± 2	162 ± 3
θ_W^* (°)	74 ± 2	63 ± 3	71 ± 1	64 ± 2	76 ± 1	150 ± 2

this study. Optimal contact angles of the water θ_W^* droplets were introduced for references. The surfaces exhibited contact angle values ranging in hydrophilic, hydrophobic and super hydrophobic regimes. On the other hand, it is worth mentioning different values of θ^* for water and blood droplets on the same functionalized surface indicating the dependence of the surface-liquid tensions on physicochemical properties of the blood. The polished metallic Si and Ti13Nb13Zr substrates without surface functionalization exhibited similar wettability with a contact angle close to 62°, characterizing a moderate hydrophilic regime. Both substrates have the ability to form an oxide layer on their surfaces. In contrast, the polymeric mushroom-like surfaces exhibited high contact angle values, in particular, a super blood-phobic regime. As can be seen, the modifications of the roughness in Ti13Nb13Zr as well as the chemical treatment on Si surfaces affect surface wetting by blood and each effect will be discussed separately in the sections 3.3, 3.4 and 3.5. The interfacial compatibility between blood and the three different substrates (Silicon, Ti13Nb13Zr and PTFE surfaces) was characterized from the determination of the interfacial free energy. In order to correlate this surface parameter with our antithrombogenic investigation, the blood-surface tension was introduced as $\gamma_{BS} = \{(\gamma_B^P)^{1/2} - (\gamma_S^P)^{1/2}\}^2 + \{(\gamma_B^d)^{1/2} - (\gamma_S^d)^{1/2}\}^2$ with polar and dispersive components of the surface free energy of the blood, $\gamma_B^P = 36.6\ mJ.m^{-2}$ and $\gamma_B^d = 11.2\ mJ.m^{-2}$, respectively [31]. In order to determine the dispersive γ_S^d and polar γ_S^P components of the substrates, dimethyl sulfoxide droplets were placed on the samples under the same experimental conditions and the free energy was calculated from polar-non polar liquids pair approaches [32,33]. From the results, the following energy values were found: γ_{BS} (PTFE) ≈ $24\ mJ.m^{-2}$, γ_{BS} (Si) ≈ $28\ mJ.m^{-2}$ and γ_{BS} (Ti13Nb13Zr) ≈ $56\ mJ.m^{-2}$. The different physicochemical properties of each kind of material explain the distinct interfacial energies. The high free energy at blood-substrate interface, as observed for Ti13Nb13Zr, is an important requirement for applications such as an antifouling material for antithrombogenic implants [34]. This surface, however, is very susceptible for chemical treatments. By way of example, the high blood-surface tension of the Ti13Nb13Zr can be drastically decreased to values close to $7\ mJ.m^{-2}$ with θ close to 35° through a simple NaOH treatment, which is the result of an increase in the oxide content on its surface and can allow adhesion components of whole blood components. Therefore, physicochemical analysis of the bloodstain rings as function of chemical modification of substrate can offer important information towards development of biomarkers and/or implant's surface.

3.2. Physicochemical characterization of the bloodstain rings

Fig. 3.a display an image of a dried blood droplet on commercial Silicon surface Si and three molecular spectra obtained from different regions of the droplet. The different localization of the peaks indicate a separation of the blood phases during evaporation process. Nevertheless, we chose not to further analyze all regions here, in terms of chemical differences, and resort to the stain rings for reasons of interest, as it provides a better comprehension of SW phenomenology in terms of contact line behavior and possible applications in medical diagnostic. Fig. 3.b shows a typical image of the bloodstain rings at the contact line (region of interest) after droplets spread-dried on the commercial Silicon surface Si investigated by confocal microscopy. The size of the stain rings was found to be around 90 μm and the molecular

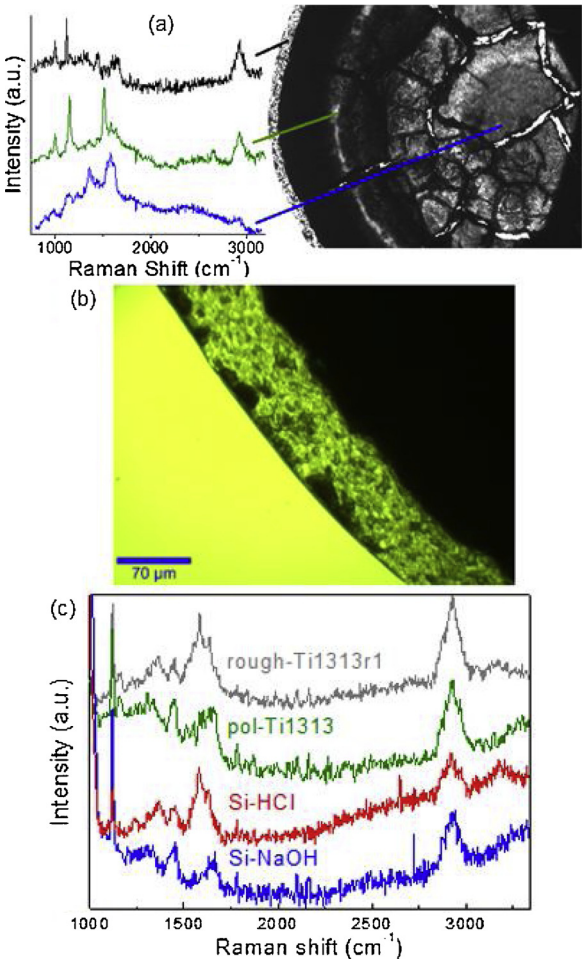

Fig. 3. Optical image of a blood droplet dried on commercial Si surface and three molecular spectra obtained from different regions of the droplet (a); Typical confocal image of a blood stain ring for spectroscopic analysis (b); and Raman spectrum on different surfaces of Silicon Si and Titanium alloy Ti13Nb13Zr. Spectra were obtained from laser with wavelength of 514 nm (c).

fingerprints of their compounds were characterized using Raman spectroscopy. During the drying process, the blood evaporation process left behind biomolecules with thick edges along the interface, that is, the "coffee ring effect" [35]. The blood stain ring effects were revealed and characterized in all surfaces, except Mus-PTFE due to a suppression of the stain ring in a super-blood-phobic state as will be discussed in Section 3.5. Fig. 3.c displays the Raman spectra of the molecular fingerprints of the contact line (ring) on Si and Ti13Nb13Zr surfaces in the range between 1000 and $3500\ cm^{-1}$. The spectra exhibited characteristic bands of the hemoglobin macromolecular structure, regardless of the red blood cells (up to > 95% of the dried weight) [36]. The principal chemical compounds of blood are hemoglobin and plasma, composed of three main protein groups: the albumins, globulins, and fibrinogens. The main molecular structures observed in bands around $1000\ cm^{-1}$ are amino acid contents in the contact line of blood on the surfaces [36]. The molecular structure observed in bands in the $2840 - 3000\ cm^{-1}$spectral range and assigned to C—H stretching from CH_2 and CH_3, the spectral region of phospholipidic chains, are characterized by symmetric and antisymmetric stretching modes enhanced by Fermi resonance [37]. Both erythrocytes and leucocytes exhibit bands from the CH_2 groups in this region [38]. Bands at the 1530-$1680\ cm^{-1}$ region are attributed to different local coordinates/assignments, such as $\nu(C\alpha - C_m)_{asym}$ and $\nu(C_\beta - C_\beta)$, of the hemoglobin [36] The functionalization of the surfaces appears to induce displacement of these bands, for instance, as a consequence of the chemical

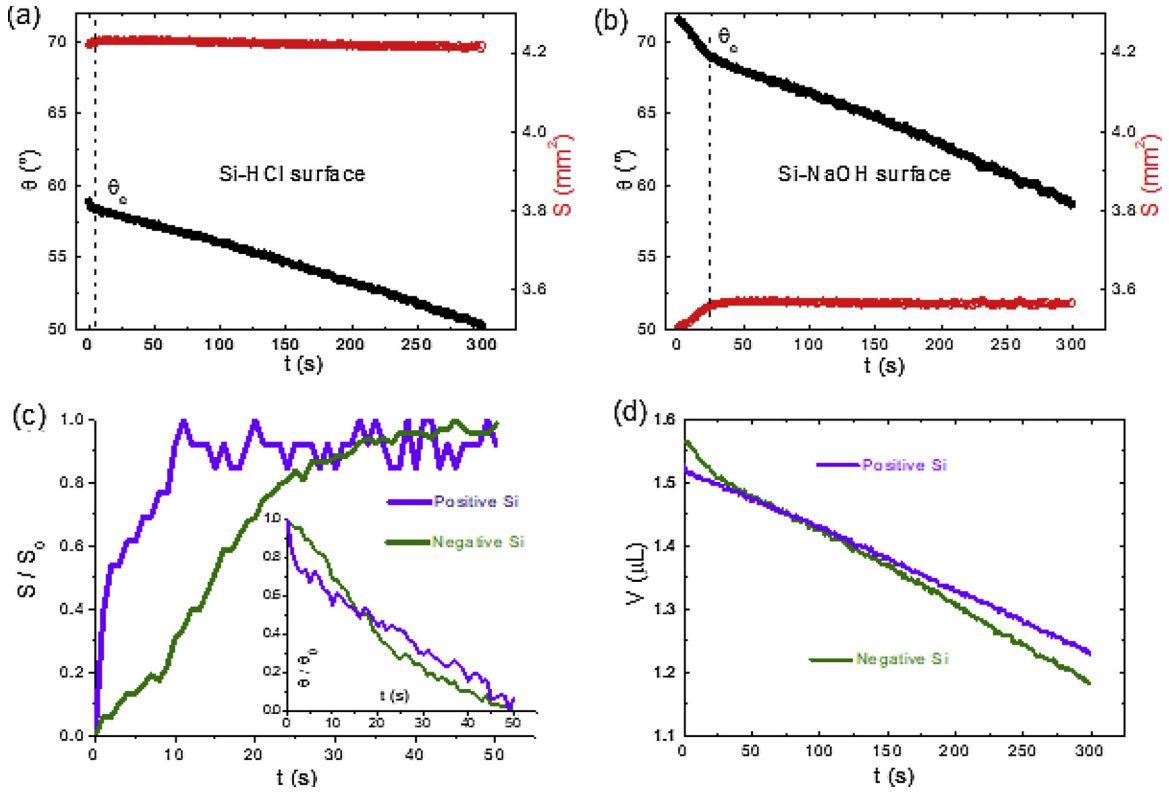

Fig. 4. Temporal evolution of contact angle θ (black) and surface area S (red) of blood droplets at 22 °C on Si − HCl (a) and Si-NaOH (b) represented in the same scale; Normalized interfacial area S/S_0 and normalized contact angle θ/θ_0 (inset) plotted against time (c) for comparisons of the wettability kinetics; Evolution of volume of the blood droplets over time on Si − HCl and Si-NaOH surfaces obtained by $V(R,\theta) = (\pi R^3).(1\text{-}\cos\theta)^2.(2+\cos\theta).(3\sin^3\theta)^{-1}$ (d). (For interpretation of the references to colour in this figure legend, the reader is referred to the web version of this article).

modification by acid and alkaline treatments, as described in the following Section.

3.3. Chemical effects

Typical wettability results of blood droplets on Si − HCl and Si-NaOH surfaces are shown in Fig. 4a–b. Just after being dripped, the blood drop advanced on the surfaces forming an interface until it reached a steady-state with $S = 4.23\,mm^2$, $3.56\,mm^2$ and $\theta_e = 58°$, 69° on Si − HCl and Si-NaOH surfaces, respectively. Fig. 4.c shows the normalized S/S_0 contact radius and the θ/θ_0 contact angle (inset) plotted against time, where S_0 is the initial interfacial area and θ_0 is the initial contact angle. The results revealed different wettability kinetics in which the movement of the contact line is delayed on the Si-NaOH. The "blood-hydrophilic" character is better observed on the positive surface as corroborated by the fast spreading of the blood and low equilibrium contact angle. Therefore, the accommodation of the drop on the surface is susceptible to chemical modification on surfaces. The evaporation process rate can be obtained from the geometrical parameters of the spherical cap by $V(r,\theta) = (\pi r^3).(1\text{-}\cos\theta)^2.(2+\cos\theta).(3\sin^3\theta)^{-1}$ over time, based on monitoring the contact angle θ and contact radius r [39]. The calculated values are displayed in the Fig. 4.d indicating different behaviors. From results, it is shown that the kinetic of evaporation exhibits remarkable dependence on the chemical treatment. The increase of the interfacial area by the acid treatment leads to a delay of the blood droplet evaporation rate. The difference in the SW by blood on Si − HCl and Si-NaOH substrates suggest that the spreading capability of the blood should be a result of different chemical interactions and/or the charge effects, since the blood cell membrane consists of phospholipid bilayers with negative charge [27].

We speculated that the SW variation for blood droplets, as presented in Fig. 4, can be attributed to different surfaces' chemistry. Thus, we further characterized the relative contributions of chemical treatments on blood components at the contact line by Raman spectroscopy. Fig. 5 shows the Raman spectra of blood stain rings on Si, Si − HCl and Si-NaOH obtained using laser source with $\lambda = 514\,nm$. Both spectra revealed high phenylalanine-aromatic amino acid contents (as observed at $1002\,cm^{-1}$) in the contact line of blood. The adsorption of this component at the contact line can be assigned to the electrostatic interaction of the terminal NH_3^+ in the amino acid with side chains containing aromatic rings. On the other hand, it is worth noticing the inversion in the intensity of the main Raman peaks $1121\,cm^{-1}$ (assigned to $\nu(C_b\text{–methyl})$) and $1530-1680\,cm^{-1}$ as a result of the chemical treatment in Si − HCl substrate. The region between $1530-1680\,cm^{-1}$ is attributed to different local coordinates/assignments, as observed after decomposition to line shape analyses of the Raman spectra (Fig. 5.b) and appears to be susceptible to interactions with different surfaces' groups. Slightly displacements in localization were noted in comparison with reference [36] indicating modification in energy bonding. In addition, the band at the $1581\,cm^{-1}$, related to cells in an oxygenated state [40], is highly affected by acid treatment of the substrates in comparison with the alkaline treatment. The bands assigned to vibrations of aromatic-amino acids (C_α-C_m asymmetric stretching) for the main protein structures from blood, such as phenylalanine, tyrosine and tryptophan can be found at this region of the spectrum. Thus, we can also speculate about the protein as a chemical effector on SW. As mentioned, one of the chemical compounds of blood is fibrinogen (factor I), a glycoprotein that is converted enzymatically by the thrombin to fibrin and subsequently to a fibrin-based blood clot during vascular injury [41]. The primary function is to occlude blood vessels and thereby stop excessive bleeding, in or case assessed, via SW. Probably, this protein has more effect to adhesion of the bloodstain rings at the contact line after droplets spread-dried process, suggesting that chemical treatments on the substrate could both separate blood

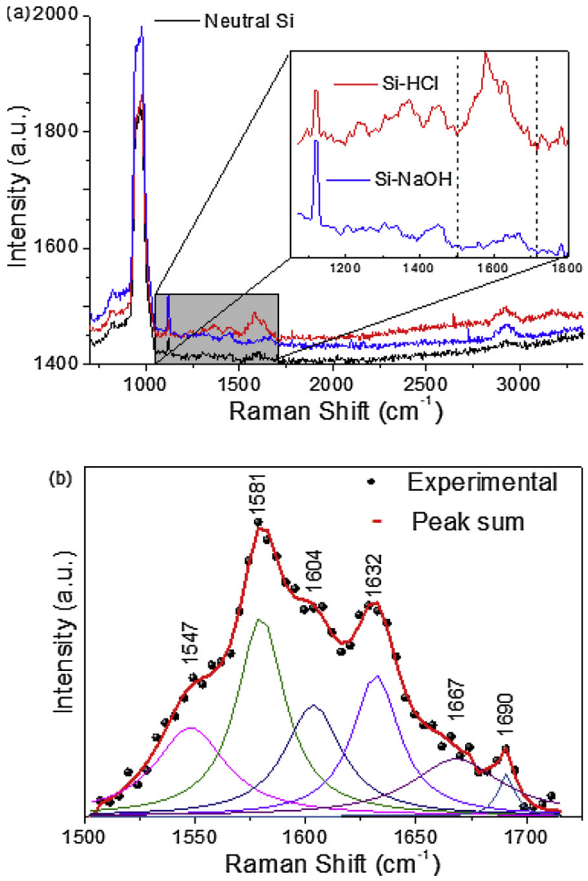

Fig. 5. Raman spectrum of blood stain rings on Si, Si−HCl (Si^+) and Si-NaOH (Si^-) obtained by using wavelength of 514 nm (a); Line shape analyses of the Raman spectra (b).

components by protein adhesion and modulate the movement of molecules during blood spreading. There is a possible implication in medical diagnostics: different methods for the cleaning of substrates based on chemical treatment could imply in different blood separation on surfaces using the same patient's blood sample.

3.4. Roughness effects

As aforementioned, the high free energy at blood-substrate interface, as observed for Ti13Nb13Zr with γ_{BS} (Ti13Nb13Zr) ≈ 56 mJ.m^{-2} could be an interesting option for applications in antithrombogenic metallic implants. However, this surface is very susceptible to chemical treatments due to increasing oxide content on its surface, necessitating more accurate and appropriate surface functionalization without chemical treatments. Figs. 6a–b shows details of the morphologies of the polished and thinned Ti13Nb13Zr obtained by AFM. From the surface profiles, the roughness parameters were obtained and the values are reported in Table 2. According to the results, the abrasion process profoundly affects the topology of the Ti13Nb13Zr increasing all roughness parameters. For instance, the relations between the polished and rough surfaces obtained for average roughness and root mean squared are Ra (Ti13Nb13Zr-r1) ≈ 5.7 Ra (Ti13Nb13Zr) and R_q (Ti13Nb13Zr-r1) ≈ 5.5 R_q (Ti13Nb13Zr), respectively. We have shown that roughness affected both blood and water contact angle, independently of its physicochemical properties (Table 1). It is relevant to highlight that other tried methods, such as abrasion by SiC, have failed to increase hydrophobicity/bloodphobicity in this metallic substrate. The topologic features of Ti and its alloy have a meaningful contribution to the biological environment response. For instance, the adsorption of blood proteins, adhesion and activation of platelets on titanium alloy implants can result in thrombus formation and inflammatory responses [14,42]. Sona Moradi and co-authors showed that in the hydrophilic regime, a higher roughness corresponds to increased blood-solid contact resulting in more platelet adhesion [43]. On the other hand, there is no quantitative data concerning the retention-adhesion forces. Herein, the adhesion was investigated by measuring the rupture of the blood meniscus θ_{rup}, in which the values were found to be 22.0 ± 7.8 and 27.0 ± 4.4 mN.m^{-1} for Ti13Nb13Zr and Ti13Nb13Zr-r1, respectively. Accounting the error bar, there is no significant difference between the adhesion surfaces at interface. The work of adhesion between blood and Ti13Nb13Zr, defined as $W = \gamma_B(\cos\theta_{rup} + 1)$, was determined and the values obtained were ≈ 91 mJ·m^{-2}. We also investigated engineering aspects of the Ti13Nb13Zr surfaces with regards to friction contributions to dynamic wetting properties. Based on advancing θ_a and receding θ_r contact angle measurements, two parameters were determined: the dynamic contact angle hysteresis, $\Delta\theta_{dyn}$, and the pinning force (per unit length), defined as $F_{dyn} = \gamma(\cos\theta_r - (\cos\theta_a + \cos\theta_r).2^{-1})$ [44]. The values obtained for Ti13Nb13Zr-r1 were slightly lower than those of Ti13Nb13Zr. Considering these dynamic wetting aspects and the increase in contact angle after the surface functionalization indicate that blood do not completely penetrate into the rough grooves on Ti13Nb13Zr-r1, that is, a non-homogeneous wetting. The hydrophobic characteristic of the rough-Ti1313-r1 surface abraded by 9 μm Alumina (Al_2O_3) associated with its low blood adhesion can be an interesting option for applications when a poor protein/cell-adhesion is required, for example, to avoid thrombotic responses at local site of the microstructures.

3.5. Fakir effect

A high suppression of the "blood stain ring" effects was observed on the bio-inspired surface. Therefore, the molecular spectra have not been detectable. Fig. 7 shows an electronic microscopic image of the bio-inspired surface (a) and a typical wetting regime of the blood on the bioinspired surface measured by the evolution of the contact angle and contact radius over time in the full hydrophobic regime (b). The blood droplets remained suspended on top of the surfaces clearly indicating a "fakir" state with constant contact angle and a decreasing in the contact area due to evaporation of the water droplet. It is interesting to note the differences in the dynamics of the interfacial area S_i and contact angle θ in comparison with the patterned Silicon substrate of Fig. 2 with values similarly scaled. The large contact angles of 150° and 160° for water and blood droplets, respectively, indicate that the blood drop does not significantly penetrate into the microstructure. Such a property could reduce protein adsorption that leads to platelet adhesion and thrombi generation since the cell detachment tends to be favored on these surfaces. In addition, the stability of the contact angle associated with the motion of the contact line is of critical importance for an optimal designing of micro fluid blood drop-based devices.

The fakir configuration of the blood droplets on the bio-inspired surfaces can open new horizons for potential applications in blood-microfluidic devices and biomarkers. In order to well describe this notable configuration, the attributes of the blood contact angle stability on the bioinspired-like surface were assessed by applying a simple physical model based on the spherical cap, phase fractions, interfacial energies and boundary conditions. The description of the system free energy (F) between blood droplets and Mush-like surfaces, the can be given by:

$$F = VE_i + S_B\gamma_B + S_i(\gamma_i - \gamma_s) + S_S\gamma_S \quad (1)$$

where V, S_B, S_S, and S_i are the volume of blood droplet, blood surface area, solid surface area and blood-surface interfacial area, respectively, while E_i, γ_S, γ_B and γ_i are the internal energy of the droplet, solid surface energy, blood surface energy and interfacial energy, respectively. A circular contact line associated to an ideal surface, which is smooth, homogeneous, isotropic, and non-deformable, can be written as:

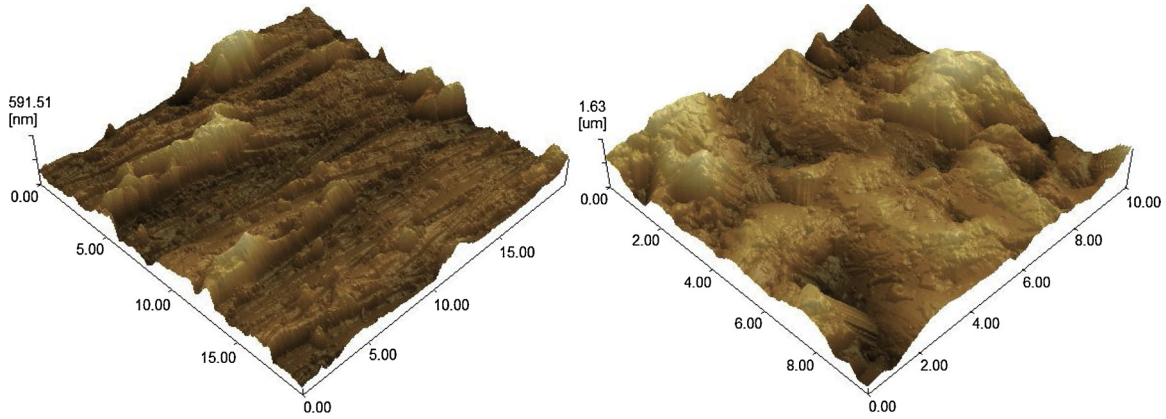

Fig. 6. AFM micrographs showing 3D view of the surfaces Ti13Nb13Zr (a) and Ti13Nb13Zr-r1 (b).

Table 2
Topological characterization of Ti13Nb13Zr substrates: roughness parameters obtained by AFM.

Surface / Roughness Parameters	Ti13Nb13Zr	Ti13Nb13Zr-r1
R_a (nm)	56	320
R_q, R_{RMS} (nm)	77	421
R_p (nm)	412	1678
R_v (nm)	179	1520
R_z (nm)	591	3197
R_{zjis} (nm)	294	1520

$$S_i.\ \gamma_i = 2\pi R^2 \sin^2\theta\gamma_i \quad (2)$$

However, in our study system, the surface is not homogeneous, since the surfaces are decorated with micrometer-sized mushroom-like pillars on a regular square lattice characterized by a gap between pillars (see details in Fig. 7.a) resulting in a blood-solid contact fraction f_{BS} and a blood-gas contact fraction f_{BG}. Therefore, we can express Eq. (2) by:

$$S_i.\ \gamma_i = S_i(\gamma_{BS}f_{BS} + \gamma_B f_{BG}) \quad (3)$$

Writing expression (1) as a function of θ and R, as described by a spherical cap, i.e., $F = F(\theta, R)$ which holds the necessary condition for the minimization of the energy ($\delta F/\delta\theta = 0$ and $\delta F/\delta R = 0$) at the optimal contact angle θ^* (steady-state). Then, the minimization of energy results can be expressed by:

$$\gamma_S{}^* = \gamma_{BS}f_{BS} + \gamma_B(\cos\theta^* - f_{BS} + 1) \quad (4)$$

Eq. (4) describes the interfacial energies of a blood droplet on surfaces in a steady state taking into account the blood-solid contact fraction. $\gamma_S{}^*$ is an apparent surface free energy since the interface involves a heterogeneous surface [45]. In order to further challenge the theoretical prediction of the optimal contact angle θ^* in the fakir state, we have introduced the Chibowski equation $\gamma_S{}^* = \gamma_L(1 + \cos\theta_a)^2(2 + \cos\theta_r + \cos\theta_a)^{-1}$, that correlates the dynamic wetting properties with apparent solid tension [46,47]. Then, we have introduced experimental values of advancing θ_a and receding θ_r contact angle of water droplets on the superhydrophobic surfaces from reference [29]. For this decorated surface, the micrometer-sized mushroom-like pillars on a regular square lattice have a gap between pillars equal to 8.2 μm (see details in Fig. 7.b) resulting in a blood-solid contact fraction f_{BS} equal to 0.19. The value of $\gamma_S{}^*$ equal to 1.7 mJ/m^2 was obtained from Chibowski equation while the value of γ_{BS} equal to 24 mJ.m^{-2} was obtained from section 3.1. For the theoretical θ^* of the Eq. (8), the following value was obtained: $\theta^* = 150°$, which has a good agreement with the experimental contact angle values measured for Mushroom-like surface (Table 1). This wetting regime is characteristic of a heterogeneous surface which could be modeled by the Cassie-Baxter equation [48]. Therefore, the super-blood-hydrophobic regime observed in this bio-inspired mushroom-like surface can be described by simple modeling based on the minimization of free energy (including phase fraction at interfaces) for predicting stable fakir effects in blood drop-based devices.

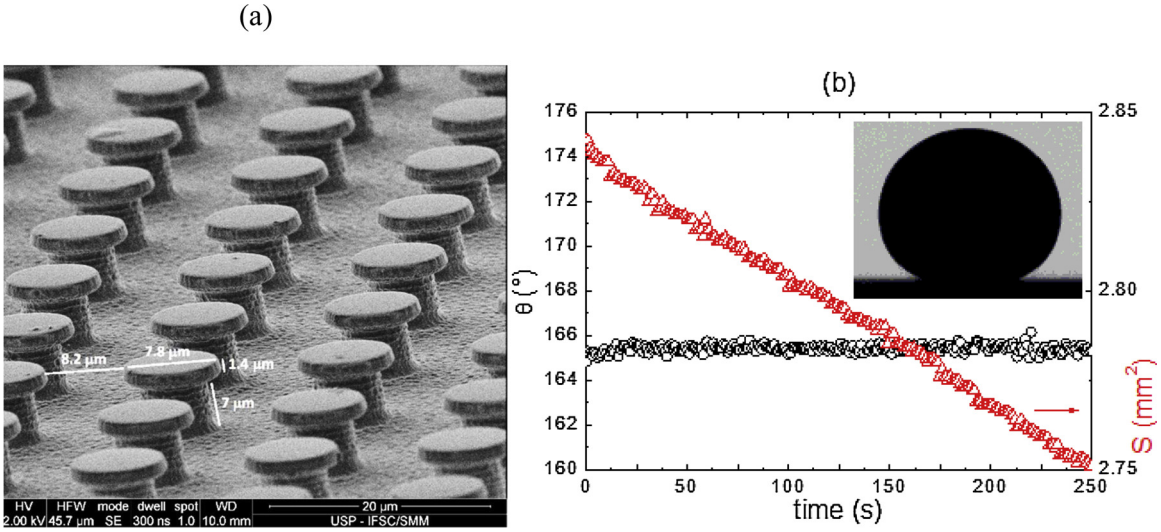

Fig. 7. Electronic microscopic image of the bio-inspired surface (a) and typical evolution of the contact angle and contact line in function of the time of a blood droplet on the surface. Inset: respective profile of the drop on surface ($\theta^* = 165°$) (b).

4. Conclusion

Blood droplets on functionalized surfaces were investigated in order to assess the phenomenology of the blood-substrate interface, in particular, chemical, topological and superhydrophobic effects. The contact angle variation was attributed to different surface' chemistry and topology. The relative contributions of surface charge (as a marker of chemical potential) and roughness (as a marker of topology) to blood spreading-dying process were further characterized. The spreading of blood droplets on the substrates followed to evaporation process left behind biomolecules with thick edges along the interface ("coffee ring effect") and its chemical components were identified by Raman spectroscopy, proving to be an useful technique in blood stain rings studies. The blood contact line is influenced by a hydrophilic-superhydrophobic range, which in turn depends on the characteristics of the surfaces (material-type dependent). The chemical modification on the surfaces by acid treatment increased the blood wettability and such effect has been attributed to the electrostatic interaction between the positive charged Si surface and the negative phospholipid bilayers of the cell membrane. We recommend that future experimental studies of surfaces for blood-material studies aiming towards substrates for disease diagnosis take chemical treatment effects into account. The increase in roughness parameters on Ti13Nb13Zr substrate decreased the hydrophilicity and provided a bloodphilic-phobic transition. This characteristic associated with low blood adhesion can be an interesting option for metallic implant applications when a poor protein/cell-adhesion is required, as, for example, to avoid thrombotic responses at the local site of the microstructures. The remarkable stability of the super blood phobic state on the bio-inspired surfaces with contact angle values close to 160° can open new horizons for potential applications in blood-microfluidic devices and biomarkers. A simple thermodynamic modeling can be applied in this surface in order to well characterize the stability of the blood-surface interface and predict optimized surface free energy (or contact angle).

Funding

This work was supported by the Fundação de Amparo à Pesquisa do Estado de São Paulo, FAPESP, Brazil, grant 2013/21970-8.

Acknowledgements

The authors thank the Growth of Crystals and Ceramic Materials CCMC team and Faculdade de Filosofia, Ciencias e Letras FFCLRP of the University of São Paulo-USP for AFM images and are indebted to prof. Dr. Rachid Rahouadj of the Université de Lorraine and Lilian Reschini of the São Francisco analyze center for all support in the theoretical modelling and blood manipulation, respectively, and also prof. Dr Christophe Pirat and prof. Dr Stella Ramos for providing the superhydrophobic substrate.

Appendix A. Supplementary data

Supplementary material related to this article can be found, in the online version, at doi:https://doi.org/10.1016/j.colsurfa.2019.04.025.

References

[1] L. Bahmani, M. Neysari, M. Maleki, The study of drying and pattern formation of whole human blood drops and the effect of thalassaemia and neonatal jaundice on the patterns, Colloids Surf. A Physicochem. Eng. Asp. 513 (2017) 66–75, https://doi.org/10.1016/j.colsurfa.2016.10.065.

[2] S.H. Chen, Y. Chang, K. Ishihara, Reduced blood cell adhesion on polypropylene substrates through a simple surface zwitterionization, Langmuir 33 (2017) 611–621, https://doi.org/10.1021/acs.langmuir.6b03295.

[3] T.C. Chao, A. Trybala, V. Starov, D.B. Das, Influence of haematocrit level on the kinetics of blood spreading on thin porous medium during dried blood spot sampling, Colloids Surf. A Physicochem. Eng. Asp. 451 (2014) 38–47, https://doi.org/10.1016/j.colsurfa.2014.03.033.

[4] D. Brutin, B. Sobac, B. Loquet, J. Sampol, Pattern formation in drying drops of blood, J. Fluid Mech. 667 (2011) 85–95, https://doi.org/10.1017/S0022112010005070.

[5] L. Richert, F. Variola, F. Rosei, J.D. Wuest, A. Nanci, Adsorption of proteins on nanoporous Ti surfaces, Surf. Sci. 604 (17–18) (2010) 1445–1451, https://doi.org/10.1016/j.susc.2010.05.007.

[6] T.C. Chao, O.A. Tash, D.B. Das, V. Starov, Simultaneous spreading and imbibition of blood droplets over porous substrates in the case of partial wetting, Colloids Surf. A Physicochem. Eng. Asp. 505 (2016) 9–17, https://doi.org/10.1016/j.colsurfa.2015.10.056.

[7] W.B. Zeid, J. Vicente, D. Brutin, Influence of evaporation rate on cracks' formation of a drying drop of whole blood, Colloids Surf. A Physicochem. Eng. Asp. 432 (2013) 139–146, https://doi.org/10.1016/j.colsurfa.2013.04.044.

[8] B. Sobac, D. Brutin, Desiccation of a sessile drop of blood: cracks, folds formation and delamination, Colloids Surf. A Physicochem. Eng. Asp. 448 (2014) 34–44, https://doi.org/10.1016/j.colsurfa.2014.01.076.

[9] W.B. Zeid, D. Brutin, Effect of relative humidity on the spreading dynamics of sessile drops of blood, Colloids Surf. A Physicochem. Eng. Asp. 456 (2014) 273–285, https://doi.org/10.1016/j.colsurfa.2014.05.004.

[10] C.R. Hsiao, C.W. Lin, C.M. Chou, C.J. Chung, J. Liang, Surface modification of blood-contacting biomaterials by plasma-polymerized superhydrophobic films using hexamethyldisiloxane and tetrafluoromethane as precursors, Appl. Surf. Sci. 346 (2015) 50–56, https://doi.org/10.1016/j.apsusc.2015.03.208.

[11] K. Fedorov, C. Blaszykowski, S. Sheikh, A. Reheman, A. Romaschin, H. Ni, M. Thompson, Prevention of thrombogenesis from whole human blood on plastic polymer by ultrathin monoethylene glycol silane adlayer, Langmuir 30 (11) (2014) 3217–3222, https://doi.org/10.1021/la500745p.

[12] S. Alibeik, S. Zhu, J.W. Yau, J.I. Weitz, J.L. Brash, Surface modification with polyethylene glycol–corn trypsin inhibitor conjugate to inhibit the contact factor pathway on blood-contacting surfaces, Acta Biomater. 7 (2011) 4177–4186, https://doi.org/10.1016/j.actbio.2011.07.022.

[13] D.E. Heath, S.L. Cooper, Design and characterization of PEGylated terpolymer biomaterials, J. Biomed. Mater. Res. 94A (2010) 1294–1302, https://doi.org/10.1002/jbm.a.32811.

[14] L.C. Xu, J. Bauer, C.A. Siedlecki, Proteins, platelets, and blood coagulation at biomaterial interfaces, Colloids Surf. B Biointerfaces 124 (2014) 49–68, https://doi.org/10.1016/j.colsurfb.2014.09.040.

[15] Z. Zhang, M. Zhan, S. Chen, T.A. Horbett, B.D. Ratner, S. Jiang, Blood compatibility of surfaces with superlow protein adsorption, Biomaterials 29 (2008) 4285–4291, https://doi.org/10.1016/j.biomaterials.2008.07.039.

[16] L. Chen, D. Han, L. Jiang, On improving blood compatibility: from bioinspired to synthetic design and fabrication of biointerfacial topography at micro/nano scales, Colloids Surf. B Biointerfaces 85 (2011) 2–7, https://doi.org/10.1016/j.colsurfb.2010.10.034.

[17] F. Rupp, R.A. Gittens, L. Scheideler, A. Marmur, B.D. Boyan, Z. Schwartz, J.G. Geis-Gerstorfer, A review on the wettability of dental implant surfaces I: theoretical and experimental aspects, Acta Biomater. 10 (2014) 2894–2906, https://doi.org/10.1016/j.actbio.2014.02.040.

[18] R.A. Gittens, L. Scheideler, F. Rupp, S.L. Hyzy, J. Geis-Gerstorfer, Z. Schwartz, B.D. Boyan, A review on the wettability of dental implant surfaces II: biological and clinical aspects, Acta Biomater. 10 (2014) 2907–2918.

[19] J.H. Park, C.E. Wasilewski, N. Almodovar, R.O. Navarrete, B.D. Boyan, R. Tannenbaum, Z. Schwartz, The responses to surface wettability gradients induced by chitosan nanofilms on microtextured titanium mediated by specific integrin receptors, Biomaterials 33 (2012) 7386–7393, https://doi.org/10.1016/j.biomaterials.2012.06.066.

[20] J.I. Rosales-Leal, M.A. Rodríguez-Valverde, G. Mazzaglia, P.J. Ramón-Torregrosa, L. Díaz-Rodríguez, O. García-Martínez, M. Vallecillo-Capilla, C. Ruiz, M.A. Cabrerizo-Vílchez, Effect of roughness, wettability and morphology of engineered titanium surfaces on osteoblast-like cell adhesion, Colloids Surf. A Physicochem. Eng. Asp. 365 (2010) 222–229, https://doi.org/10.1016/j.colsurfa.2009.12.017.

[21] A. Ranella, M. Barberoglou, S. Bakogianni, C. Fotakis, E. Stratakis, Tuning cell adhesion by controlling the roughness and wettability of 3D micro/nano silicon structures, Acta Biomater. 6 (2010) 2711–2720, https://doi.org/10.1016/j.actbio.2010.01.016.

[22] Y. Li, Y. Wei, J. Liao, Y. Hao, C. Ning, L. Jiang, S. Wang, Surface wettability switched cell adhesion and detachment on conducting polymer nano array, Adv. Mater. Interfaces 3 (2016) 1600598, , https://doi.org/10.1002/admi.201600598.

[23] G. Zhao, A. Raines, M. Wieland, Z. Schwartz, B.D. Boyan, Requirement for both micro-and submicron scale structure for synergistic responses of osteoblasts to substrate surface energy and topography, Biomaterials 28 (2007) 2821–2829, https://doi.org/10.1016/j.biomaterials.2007.02.024.

[24] M. Nakamura, A. Nagai, T. Hentunen, J. Salonen, Y. Sekijima, T. Okura, K. Hashimoto, Y. Toda, H. Monma, K. Yamashita, Surface electric fields increase osteoblast adhesion through improved wettability on hydroxyapatite electret, ACS Appl. Mater. Interfaces 1 (10) (2009) 2181–2189, https://doi.org/10.1021/am900341v.

[25] N.J. Hallab, K.J. Bundy, K. O'Connor, R.L. Moses, J.J. Jacobs, Evaluation of metallic and polymeric biomaterial surface energy and surface roughness characteristics for directed cell adhesion, Tissue Eng. 7 (2001) 55, https://doi.org/10.1089/107632700300003297.

[26] M.P. Molina, P.G. Moreno, J.E.F. Barbero, F. O'Valle, A.B.J. Reyes, J.L.O. Vinuesa, P.J.R. Torregrosa, Role of wettability and nanoroughness on interactions between osteoblast and modified silicone surfaces, Acta Biomater. 7 (2011) 771–778,

https://doi.org/10.1016/j.actbio.2010.08.024.
[27] K. Xiao, Y. Li, J. Luo, J.S. Lee, W. Xiao, A.M. Gonik, R.G. Agarwal, K.S. Lam, The effects of surface charge on in vivo biodistribution of PEG-oligocholic acid based micellar nanoparticles, Biomaterials 32 (2011) 3435–3446, https://doi.org/10.1016/j.biomaterials.2011.01.021.
[28] R.M. do Nascimento, V.R. Carvalho, J.S. Govone, A.C. Hernandes, N.C. Cruz, Effects of negatively and positively charged Ti metal surfaces on ceramic coating adhesion and cell response, J. Mater. Sci. Mater. Med. 28 (2017) 33, https://doi.org/10.1007/s10856-017-5848-0.
[29] R.M. Nascimento, C. Cottin-Bizonne, C. Pirat, S.M.M. Ramos, Water drop evaporation on mushroom-like superhydrophobic surface: temperature effects, Langmuir 32 (8) (2016) 2005–2009, https://doi.org/10.1021/acs.langmuir.5b04445.
[30] R.M. Nascimento, S.M. Ramos, I.H. Bechtold, A.C. Hernandes, Wettability Study on Natural Rubber Surfaces for Applications as Biomembranes, ACS Biomater. Sci. Eng. 8 (2018) 2784–2793, https://doi.org/10.1021/acsbiomaterials.8b00723.
[31] J.Y. Chen, Y.X. Leng, X.B. Tian, L.P. Wang, N. Huang, P.K. Chu, P. Yang, Antithrombogenic investigation of surface energy and optical bandgap and hemocompatibility mechanism of Ti (Ta^{+5})O_2 thin films, Biomaterials 23 (2002) 2545–2552, https://doi.org/10.1016/S0142-9612(01)00389-1.
[32] D.K. Owens, R.C. Wendt, Estimation of the surface free energy of polymer, J. Appl. Polym. Sci. 13 (1969) 1741–1747, https://doi.org/10.1002/app.1969.070130815.
[33] D.H. Kaelble, Dispersion-polar surface tension properties of organic solids, J. Adhes. 2 (1970) 66–81, https://doi.org/10.1080/0021846708544582.
[34] X. Liu, L. Yuan, D. Li, Z. Tang, Y. Wang, G. Chen, H. Chen, J.L. Brash, Blood compatible materials: state of the art, J. Mater. Chem. B 2 (2014) 5718–5738, https://doi.org/10.1039/C4TB00881B.
[35] R.D. Deegan, O. Bakajin, T.F. Dupont, G. Huber, S.R. Nagel, T.A. Witten, Capillary flow as the cause of ring stains from dried liquid drops, Nature 389 (1997) 827–829, https://doi.org/10.1038/39827.
[36] C.G. Atkins, K. Buckley, M.W. Blades, R.F.B. Turner, Raman spectroscopy of blood and blood components, Appl. Spectrosc. 0 (0) (2017) 1–27, https://doi.org/10.1177/0003702816686593.
[37] B.P. Gaber, W.L. Peticolas, On the quantitative interpretation of biomembrane structure by Raman spectroscopy, Biochim. Biophys. Acta 465 (1977) 260–274, https://doi.org/10.1016/0005-2736(77)90078-5.
[38] E.A. Carter, K.K. Tam, R.S. Armstrong, P.A. Lay, Vibrational spectroscopic mapping and imaging of tissues and cells, Biophys. Rev. 1 (2) (2009) 95–103, https://doi.org/10.1007/s12551-009-0012-9.
[39] H.Y. Erbil, G. McHale, M.I. Newton, Drop evaporation on solid surfaces: constante contact angle mode, Langmuir 18 (2002) 2636–2641, https://doi.org/10.1021/la011470p.
[40] G. Perozziello, P. Candeloro, A. De Grazia, F. Esposito, M. Allione, M.L. Coluccio, R. Tallerico, I. Valpapuram, L. Tirinato, G. Das, A. Giugni, B. Torre, P. Veltri, U. Kruhne, G.D. Valle, E.D. Fabrizio, Microfluidic device for continuous single cells analysis via Raman spectroscopy enhanced by integrated plasmonic nanodimers, Opt. Express 24 (2) (2016) A180–A190, https://doi.org/10.1364/OE.24.00A180.
[41] K.W.C. Poon, F.M. Lyng, P. Knief, O. Howe, A.D. Meade, J.F. Curtin, H.J. Byrne, J. Vaughan, Quantitative reagent-free detection of fibrinogen levels in human blood plasma using Raman spectroscopy, Analyst 137 (2012) 1807–1814, https://doi.org/10.1039/c2an35042d.
[42] Z.M. Ruggeri, Mechanisms initiating platelet thrombus formation, Thromb. Haemost. 78 (1997) 611–616, https://doi.org/10.1055/s-0038-1657598.
[43] S. Moradi, N. Hadjesfandiari, S.F. Toosi, J.N. Kizhakkedathu, S.G. Hatzikiriakos, Effect of extreme wettability on platelet adhesion on metallic implants: from superhydrophilicity to superhydrophobicity, ACS Appl. Mater. Interfaces 8 (27) (2016) 17631–17641, https://doi.org/10.1021/acsami.6b03644.
[44] J.F. Joanny, P.G. de Gennes, A model for contact angle hysteresis, J. Chem. Phys. 81 (1984) 552–562, https://doi.org/10.1063/1.447337.
[45] J. Bico, C. Marzolin, D. Quéré, Pearl drops, Europhys. Lett. 47 (2) (1999) 220–226 https://iopscience.iop.org/article/10.1209/epl/i1999-00453-y.
[46] E. Chibowski, On some relations between advancing, receding and Young's contact angles, Adv. Colloid Interface Sci. 133 (2007) 51, https://doi.org/10.1016/j.cis.2007.03.002.
[47] E. Chibowski, Apparent surface free energy of superhydrophobic surfaces, J. Adhes. Sci. Technol. 25 (12) (2011) 1323–1336, https://doi.org/10.1163/016942411X555890.
[48] E. Bormashenko, Why does the Cassie-Baxter equation apply? Colloids Surf. A: Physicochem. Eng. Asp. 234 (2008) 47–50, https://doi.org/10.1016/j.colsurfa.2008.03.025.

Glossary

F: system free energy (mJ.m^{-2})
f_{BS}: blood-solid contact fraction
f_{BG}: blood-gas contact fraction
γ_i: interfacial free energy (mJ.m^{-2})
γ_B: blood surface free energy (mJ.m^{-2})
E_i: internal energy of the droplet (mJ.m^{-3})
γ_s: surface free energy of the substrate (mJ.m^{-2})
$\gamma_s{}^*$: apparent surface free energy of the substrate (mJ.m^{-2})
$\gamma_s{}^p$: polar component of the surface free energy of the substrate (mJ.m^{-2})
$\gamma_s{}^d$: dispersive component of the surface free energy of the substrate (mJ.m^{-2})
γ_L: surface free energy of the liquid (mJ.m^{-2})
$\gamma_l{}^p$: polar component of the surface free energy of the liquid (mJ.m^{-2})
$\gamma_l{}^d$: dispersive component of the surface tension of the liquid (mJ.m^{-2})
λ: Lagrange Multiplier
R: radius of the sphere (mm)
R_a: average roughness (nm)
R_q: root mean squared (nm)
R_p: maximum peak height (nm)
R_v: maximum valley depth (nm)
R_z: ten-point height (nm)
R_{zjis}: five highest peaks and lowest valleys (nm)
S_B: blood-surface area (mm^2)
S_S: solid surface area (mm^2)
S_i: blood-surface interfacial area (mm^2)
θ: transient contact angle (°)
θ^*: optimal contact angle steady-state (°)
V: volume of the blood droplet (mm)